2023 IEEE/ASME International Conference on Advanced Intelligent Mechatronics (AIM)
June 28-30, 2023. Seattle, Washington, USA

Actuator Placement in Adaptive Structures for Static Compensation – Minimizing Displacements versus Minimizing Actuator Forces

Fabian Friz, Amelie Zeller, Michael Böhm and Oliver Sawodny[1]

***Abstract*— Adaptive structures are equipped with sensors and actuators to counteract deformations caused by external loads. Previous work has shown that active control of high-rise buildings to compensate for static displacements and dampen vibrations can reduce resource consumption by half. In order to achieve this, proper placement of actuators is a delicate part in the design process of adaptive structures. In this paper, a general two-stage optimization procedure is proposed to place actuators for adaptive structures under static loads. Former studies focused on placing actuators to minimize displacements. However, this leads to unnecessary large actuator forces, as displacements do not have to be compensated as much as possible, but only to reach certain service criteria. For this, different objectives using the proposed optimization procedure are introduced, minimizing either the displacements or the actuator forces while maintaining displacement constraints, what should lead to a reduction in the required actuation forces. The optimization results are systematically compared for an example structure in terms of the resulting displacements, the required actuator forces and the respective optimal actuator configurations.**

I. INTRODUCTION

The construction sector is responsible for a large share of global resource consumption and greenhouse gas emissions. To minimize adverse effects of climate change while fulfilling the demand for buildings and infrastructure of the growing world population, we need to build more with less.

Adaptive structures are equipped with sensors, actuators and a control unit to counteract displacements and vibrations due to external loads, such as wind or earthquakes [1]. The world's first adaptive high-rise building D1244 was recently built at the University of Stuttgart and is depicted in Fig. 1. For stiffness-governed structures such as high-rises, a significant amount of material is not utilized for stability, but to provide sufficient stiffness to meet displacement (maximum deflection, inter-story drift) and acceleration service criteria. Adaptive structures can meet these criteria by adaptation to deformations through feedback control algorithms and thus avoid unnecessary material usage [2, 3]. Previous studies on the design and life cycle analysis of an adaptive high-rise building expect material savings of up to $50\,\%$ [4].

The actuator configuration of an adaptive structure (the number and positions of actuators), determines its ability to counteract or compensate external loads. Therefore, actuator placement methods are an important part of the design process of such structures. Often actuators shall be placed, such that some objective is minimized. Therefore, an optimization-based approach is used herein. A common objective is to place actuators such that the displacements due to external static loads are minimized [5], [6]. However, this often requires high actuator forces, undermining the aim of minimizing resources. Given the mentioned displacement and acceleration constraints, there is actually no need to minimize displacements. Instead, to reduce actuator forces, they can be minimized under the given constraints, rather than minimizing displacements. For static wind loads, this work systematically compares the optimization objectives that minimize the actuator forces under displacement constraints or that minimize the displacements.

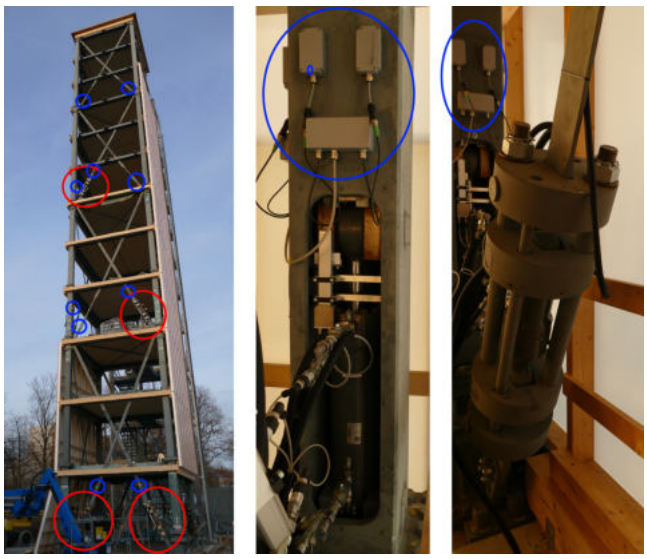

Fig. 1. Left: adaptive high-rise structure D1244 during construction with hydraulic actuators (red) and sensors as strain gauges, camera-tracked LEDs, etc. (blue). Middle and right: close-up of actuator in vertical column and diagonal bracing, respectively.

Senatore et. al [7] propose a method to design minimum energy adaptive structures due to static loads. As optimization objective serves the whole-life operational energy subject to many constraints, including the displacement constraints considered within this paper. However, the combination with additional stress and input constraints in [7] renders studying the impact of individual constraints difficult. Furthermore, the actuator configurations are not optimized, as in this paper, but chosen in advance, e. g. the set of all column actuators. With some of these chosen actuator configurations, the constraints are not reachable. Wang et. all [8] and [3] extend the approach of [7] to account for further structural design criteria and constraints. However, again the actuator configurations are not optimized, but chosen in advance. This paper aims to fill this gap, so that in a further study

*Funded by Deutsche Forschungsgemeinschaft (DFG, German Research Foundation) - Project-ID 279064222 – SFB 1244. Subproject A06.

[1] all authors are with the Institute for System Dynamics, University of Stuttgart, Stuttgart, Germany

these objectives can be combined to a simultaneous actuator placement and structural design optimization for adaptive structures. Recent literatur on optimization-based actuator placement for adaptive structures focuses on control methods based on Gramians, such as the steady-state compensability Gramian [5], a homogenizability Gramian [9] and the well-known controllability Gramian [6]. However, most of these works do not focus on realistic load cases and actuator configurations are mainly optimized for a set of unrealistic (e. g. unit-) disturbances. In this paper, we optimize for certain static wind loads and study the impact of the chosen load case on the actuator placement result and the structure's ability to compensate. So far no optimization-based actuator placement method for adaptive structures minimizes actuator forces while maintaining displacement constraints. A systematic comparison of the impact of different optimization objectives and constraints on the solution is missing as well.

The main contribution of this paper is a general two-stage formulation of an actuator placement optimization procedure, the optimization of actuator configurations such that the required actuator forces to meet displacement constraints are minimum and the systematic comparison of this objective to the common objective of minimizing the displacements. The comparison includes the actuator forces and displacements, the actuator configurations, the impact of displacement constraints and assumed loads on the results and how well actuator configurations optimized for displacement minimization perform w. r. t. actuator force minimization.

The paper is organized as follows. Section II describes the system and modeling, Section III introduces the two-stage optimization procedure and the objectives studied herein. Section IV presents and systematically compares the results obtained for the different objectives, followed by a summary and conclusion in Section V.

II. System Description and Modeling

This paper considers high-rise structures subject to static wind loads, as shown in Fig. 3 (a). A structure $\mathcal{S} = \{\mathcal{N}, \mathcal{E}\}$ consists of nodes $\mathcal{N}$ and elements $\mathcal{E}$. Each element $\mathfrak{e} \in \mathcal{E}$ is of type link or beam and has two nodes. The nodes have an appropriate number of degrees of freedom (DOFs) depending on the element type. The elements are connected at nodes thus sharing DOFs. Supports are modeled by fixating the respective DOFs. Table I contains the parameters of the 2-dimensional example structure from Fig. 3 considered herein. All remaining DOFs are collected in the vector $\boldsymbol{q} \in \mathbb{R}^n$. The static model equations are given by [10]

$$\boldsymbol{K}\boldsymbol{q} = \boldsymbol{B}\boldsymbol{u} + \boldsymbol{E}\boldsymbol{z}, \tag{1a}$$

$$\boldsymbol{y} = \boldsymbol{C}\boldsymbol{q}, \tag{1b}$$

where $\boldsymbol{K} \in \mathbb{R}^{n\times n}$ denotes the positive-definite stiffness matrix. On the right hand side, $\boldsymbol{z} \in \mathbb{R}^{n_\mathrm{z}}$ and $\boldsymbol{u} \in \mathbb{R}^r$ represent the loads and the actuator forces. The output $\boldsymbol{y} \in \mathbb{R}^{n_\mathrm{y}}$ includes e. g. element forces, elongations or displacements extracted by the output matrix $\boldsymbol{C} \in \mathbb{R}^{n_\mathrm{y}\times n}$. The input matrix $\boldsymbol{B} \in \mathbb{R}^{n\times r}$ maps the actuator forces to the DOFs. Each column in $\boldsymbol{B}$ represents the influence of a single actuator. As described in [10], various actuation concepts can be modeled by choosing $\boldsymbol{B}$ accordingly. We limit this study to a force-parallel integration of all actuators. Such actuators are modeled by two forces acting in opposite directions on the nodes of the actuated element [10] as sketched in Fig. 2.

TABLE I
Parameters of the example structure.

width	3 m	material	steel
height	30 m	wall thickness	0.01 m
num. of stories	10	cross section	0.2×0.2 m
num. of nodes	22	density	7850 kg m^{-3}
num. of elem.	50	Young's mod.	210 GPa
element type	link	Poisson's ratio	0.3
DOFs per node	x-, y-displ.	fixed DOFs	all bottom DOFs

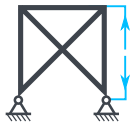

Fig. 2. Force-parallel actuation principle.

The disturbance input matrix $\boldsymbol{E} \in \mathbb{R}^{n\times n_\mathrm{z}}$ maps the loads $\boldsymbol{z}$ to the DOFs. Each column of $\boldsymbol{E}$ can be interpreted as the profile of one load and each entry of $\boldsymbol{z}$ as a load amplitude. This allows for modeling of various static loads, e. g., wind or live loads. This work considers two load cases $N_\mathrm{loads} = 2$, a static wind load from the left and one from the right. In both cases, a single load ($n_\mathrm{z} = 1$) acts on the (horizontal) x-displacement DOFs of all nodes facing the wind. Since the wind velocity increases with height, a profile increasing linearly from bottom to top is used, see Fig. 3 (a). The load amplitude is chosen such that the x-displacement of the top node at the downwind side equals is $h/100$, where h is the structure's height. The loads are collected in the set of loads $\mathcal{Z} = \{\boldsymbol{E}_i\boldsymbol{z}_i, i = 1, \ldots, N_\mathrm{loads}\}$.

When considering displacement constraints in this paper, all x-displacement DOFs of the active structure of load case i, $\boldsymbol{y}_{\mathrm{a},i}$ ($\boldsymbol{C}$ chosen accordingly), are limited to 20 % of those of the passive structure $\boldsymbol{y}_{\mathrm{p},i}$. For load cases $1, \ldots, N_\mathrm{loads}$, the feasible displacement region is thus given by

$$\mathcal{Y} = \left\{ \boldsymbol{Y} \in \mathbb{R}^{n_\mathrm{y}\cdot N_\mathrm{loads}} \;\middle|\; -|\boldsymbol{Y}_\mathrm{c}| \le \boldsymbol{Y} \le |\boldsymbol{Y}_\mathrm{c}| \right\}, \tag{2}$$

where $|\cdot|$ takes the absolute value of each vector entry and

$$\boldsymbol{Y} = [\boldsymbol{y}_{\mathrm{a},1}^\top, \ldots, \boldsymbol{y}_{\mathrm{a},N_\mathrm{loads}}^\top]^\top, \tag{3}$$

$$\boldsymbol{Y}_\mathrm{c} = 0.2 \cdot [\boldsymbol{y}_{\mathrm{p},1}^\top, \ldots, \boldsymbol{y}_{\mathrm{p},N_\mathrm{loads}}^\top]^\top. \tag{4}$$

The displacement constraints are illustrated in Fig. 3 (c).

III. Problem Statement and Actuator Placement Optimization

Employing an actuator configuration implies to apply actuator forces, which can be optimized in addition to the actuator configuration itself. To solve the actuator placement optimization problem (OP), a two-stage optimization procedure is proposed. An *outer* OP optimizes over actuator configurations, while for a given actuator configuration, the actuator forces are optimized by solving an *inner* OP, which can include constraints representing e. g., service criteria. Herein, the inner OP either minimizes actuator forces under

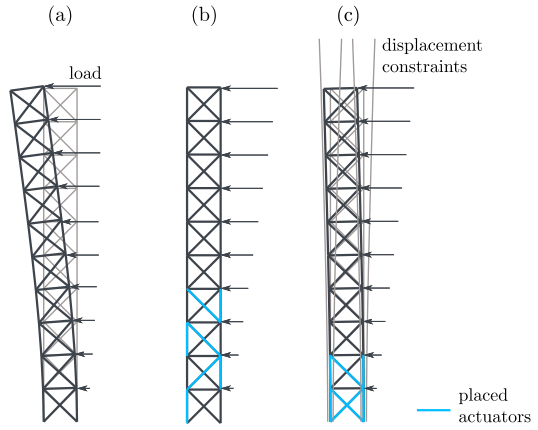

Fig. 3. Illustration of the loaded structure, which (a) is passive, (b) minimizes the displacements and (c) reduces the displacements to reach displacement constraints.

the required displacement constraints ($J_{\mathrm{U}\mathcal{Y}}$-objective), or, as previous works suggest, simply minimizes the displacements (J_{Y}-objective). To illustrate both objectives, Fig. 3 schematically depicts the resulting displacements of the structure adapting to a static wind load.

A. Actuator Placement Optimization

To formally state the actuator placement OP, let $\mathcal{E}_{\mathrm{act}} \subseteq \mathcal{E}$ be the set of elements that can be actuated and $\mathcal{S}_r \subseteq \mathcal{E}_{\mathrm{act}}$ an actuator configuration with cardinality $|\mathcal{S}_r| = r$. Note, the input matrix in (1) depends on $\mathcal{S}_r$, i. e. $\boldsymbol{B} = \boldsymbol{B}(\mathcal{S}_r)$. For all load cases, the actuator forces are collected in $\boldsymbol{U} = [\boldsymbol{u}_1^\top, \dots, \boldsymbol{u}_{N_{\mathrm{loads}}}^\top]^\top \in \mathbb{R}^{r \cdot N_{\mathrm{loads}}}$ and the resulting outputs according to (1) and (3) are collected in $\boldsymbol{Y}$. A fixed number of actuators r is placed by solving the outer OP

$$\min_{\mathcal{S}_r} J(\boldsymbol{U}^*, \boldsymbol{Y}^*) \tag{5a}$$

$$\text{s.t. } \mathcal{S}_r \in \mathcal{E}_{\mathrm{act}}, \tag{5b}$$

which yields the optimal actuator configuration $\mathcal{S}_r^*$. The cost $J(\boldsymbol{U}^*, \boldsymbol{Y}^*)$ of an actuator configuration results from the optimal actuator forces $\boldsymbol{U}^*$ and/ or displacements $\boldsymbol{Y}^*$ found by solving the inner OP

$$\min_{\boldsymbol{U},\boldsymbol{Y}} J(\boldsymbol{U}, \boldsymbol{Y}) \tag{6a}$$

$$\text{s.t. } \boldsymbol{U} \in \mathbb{R}^{r \cdot N_{\mathrm{loads}}} \tag{6b}$$

$$\boldsymbol{Y} \leftarrow (1), (3) \text{ and } \boldsymbol{E}_i \boldsymbol{z}_i \in \mathcal{Z}, i = 1, \dots, N_{\mathrm{loads}} \tag{6c}$$

$$g(\boldsymbol{U}, \boldsymbol{Y}) \leq 0. \tag{6d}$$

So the objective function is minimized for a given actuator configuration in the inner OP, and the smallest minimum is searched by the outer OP. Illustrated in Fig. 4, the optimization procedure is called a *Min-Min* problem [11]. The objective functions of the inner and outer OP do not need to be equal. However, different objective functions may lead to strange results, if the objectives are contradictory. Therefore, the same objective function is adopted here for both OPs. Any possible constraints are satisfied in both OPs, since the outer OP only evaluates solutions of the inner OP.

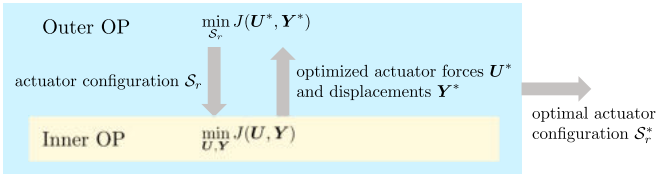

Fig. 4. Illustration of the two-stage optimization procedure.

B. Studied Objectives

The following objectives are used:

- $J_{\mathrm{Y}}(\boldsymbol{U}, \boldsymbol{Y}) = \boldsymbol{Y}^\top \boldsymbol{Y}$
  minimizes displacements without any constraints. This common objective serves as reference for comparison.
- $J_{\mathrm{U}\mathcal{Y}}(\boldsymbol{U}, \boldsymbol{Y}) = \boldsymbol{U}^\top \boldsymbol{U}$ and $\boldsymbol{Y} \in \mathcal{Y}$
  minimizes actuator forces required to stay within the displacement constraints given by (2). The constraints can be written in the form of (6d).
- $J_{\mathrm{Y}}(\boldsymbol{U}, \boldsymbol{Y}) = \boldsymbol{Y}^\top \boldsymbol{Y}$ and $\boldsymbol{Y} \in \mathcal{Y}$
  minimizes displacements within the constraints (2),
- $J_{\mathrm{UY}\mathcal{Y}}(\boldsymbol{U}, \boldsymbol{Y}) = \alpha \boldsymbol{U}^\top \boldsymbol{U} + (1-\alpha)\theta \boldsymbol{Y}^\top \boldsymbol{Y}$ and $\boldsymbol{Y} \in \mathcal{Y}$
  minimizes a weighted sum of actuator forces required to reach the displacement constraints (2) and the resulting displacements. To adjust the individual weights, $\alpha \in [0, 1]$ is used. The scaling factor $\theta \in \mathbb{R}$ aligns displacements and actuator forces to the same order of magnitude. Note that $\alpha = 0$ and $\alpha = 1$ yield the $J_{\mathrm{Y}\mathcal{Y}}$- and the $J_{\mathrm{U}\mathcal{Y}}$-objective, respectively.

C. Optimization algorithms

The inner OP (6) is classified as continuous. The solution for the J_{Y}-objective can be expressed analytically using the Moore-Penrose pseudoinverse and then evaluated numerically. For the other objectives, gradient-based optimization algorithms (Matlab fmincon) are applied. In case of the $J_{\mathrm{Y}\mathcal{Y}}$-objective, where (except for few actuators) the optimum lies within the feasible region, the algorithm option is set to interior-point. In case of the $J_{\mathrm{U}\mathcal{Y}}$- and $J_{\mathrm{UY}\mathcal{Y}}$-objectives, the algorithm option is set to active-set. All algorithms are applied with standard settings. For the $J_{\mathrm{Y}\mathcal{Y}}$-objective, where (except for few actuators) the optimum lies within the feasible region, an interior-point-method is used. For details, see [12]. The outer OP (5) is classified as combinatoric. Due to the number of actuator position candidates, not all possible actuator configurations can be tested. Previous work compared optimization algorithms for solving a combinatoric actuator placement OP for adaptive structures, where a greedy-algorithm turned out to be a good trade-off between computational effort and quality of the solution [13]. A forward or reverse greedy-algorithm begins by calculating the solution for the full or empty actuator configuration set, respectively. In the case of an empty actuator configuration set, i. e., the passive structure, the displacement constraint (if present) is violated. To avoid this, the reverse greedy is chosen. A summary of the heuristic algorithm is given here, and the reader is referred to [5], [6], or [13]. Starting with the actuator configuration including all m actuators, the algorithm removes the actuator that yields the smallest objective function increase. With $\mathcal{S}_m = \mathcal{E}_{\mathrm{act}}$, the algorithm

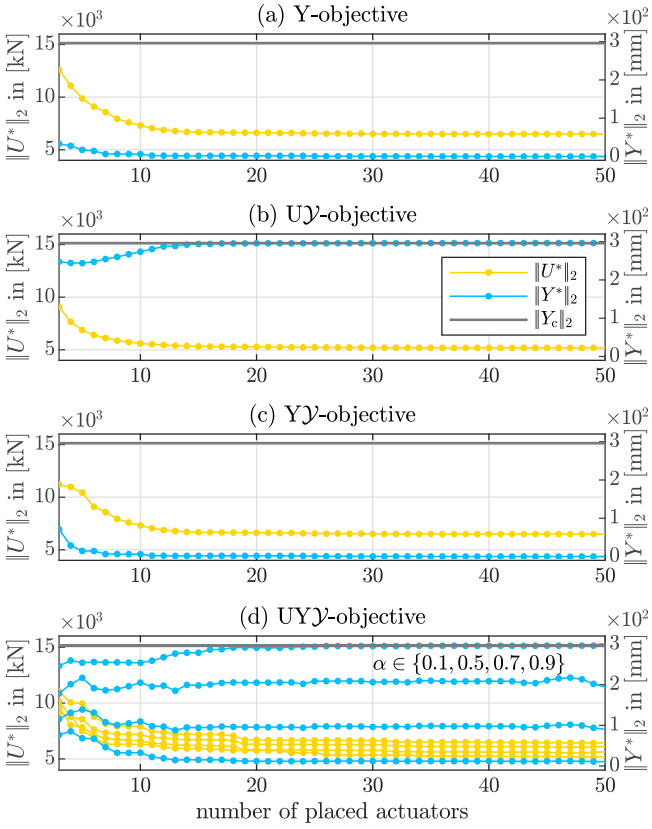

Fig. 5. Norm of optimal actuator forces and resulting displacements for the (a) Y-, (b) UY-, (c) YY- and (d) UYY-objective.

is formally stated for $r \in \{1, \dots, m-1\}$ as:

$$\mathcal{S}_{r-1} = \mathcal{S}_r \backslash \{\underset{\mathfrak{e} \in \mathcal{S}_r}{\operatorname{argmin}} \Delta J(\mathfrak{e})\}, \text{ where}$$
$$\Delta J(\mathfrak{e}) = J(\boldsymbol{U}^*(\mathcal{S}_r \backslash \mathfrak{e}), Y^*(\mathcal{S}_r \backslash \mathfrak{e})) - J(\boldsymbol{U}^*(\mathcal{S}_r), Y^*(\mathcal{S}_r)).$$

IV. Results

A desired number of actuators is placed into the example structure by solving the actuator placement OP (6), (5) w. r. t. the four objectives Y, UY, YY and UYY. The actuator placement OP is each solved for $r = 2, \dots, m$ actuators ($r = 1$ is partially not feasible, $m = 50$). Each combination of objective and number of placed actuators leads to an optimized actuator configuration $\mathcal{S}_r^*$, along with the optimized actuator forces $\boldsymbol{U}^*$ and displacements $\boldsymbol{Y}^*$. For comparison, we take their Euclidean norms

$$\|\boldsymbol{U}^*\|_2 = \frac{1}{r N_{\text{loads}}} \boldsymbol{U}^{*\top} \boldsymbol{U}^*, \quad \|\boldsymbol{Y}^*\|_2 = \frac{1}{n_y N_{\text{loads}}} \boldsymbol{Y}^{*\top} \boldsymbol{Y}^*,$$

referred to by actuator forces and displacements (norm) in the following to improve readability. To be able to compare $\|\boldsymbol{Y}^*\|_2$ to the constraints, they are also normalized to

$$\|\boldsymbol{Y}_c\|_2 = \frac{1}{n_y N_{\text{loads}}} |\boldsymbol{Y}_c|^\top |\boldsymbol{Y}_c|.$$

Note that $\|\boldsymbol{Y}_c\|_2$ is a constant value that depends on the considered loads, but on neither the objective nor the number of actuators. For the load from the right, the displacements along the downwind side of the structure (referred to by side line in the following) are depicted together with the

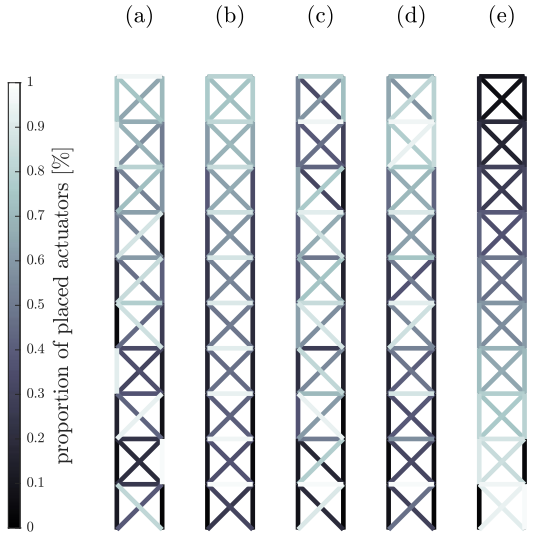

Fig. 6. Actuator configurations for the (a) Y-, (b) UY-, (c) YY- and (d) UYY-objective and (e) for the UY-objective optimized for unit loads. Dark (light) elements are contained in actuator configurations with few (many) placed actuators.

displacement constraints for this structure side. Last, the resulting actuator configurations are studied.

A. Results for the Objectives

a) Y*-Objective:* The actuator forces and displacements obtained for placing actuators using this objective are depicted in Fig. 5 (a). The displacements decrease with a growing number of actuators: they are smaller than 2.3 mm for $r > 10$ and smaller than 10^{-11} mm for $r > 39$ actuators. The actuator forces also decrease. As suggested by the small displacement norm, Fig. 7 (a) illustrates an upright side line using 12 actuators. The effects due to the load from the right are almost completely compensated. However, the side line for three placed actuators describes an S-curve slightly violating the displacement constraints in the lower part. This comes at no surprise, as they are not considered in this objective, but indicates large and undesired inter-story drift values. The resulting actuator configurations are depicted in Fig. 6 (a), where a dark (light) color means that the actuator is contained in actuator configurations with few (many) actuators. The selection of actuators seems not to follow a pattern.

b) UY*-Objective:* The actuator forces decrease for an increasing number of actuators while the displacements increase up to the normalized constraint, see Fig. 5 (b). From about 12 actuators on, the displacements are compensated only to the necessary extent, avoiding expensive overcompensation, with the required actuator forces about 40 % smaller of those calculated using the Y-objective. The side line for 12 actuators in Fig. 7 (b) matches the left displacement constraint well. This illustrates the energy savings that can be realized by the right choice of optimization objective. For three actuators, the side line stays within the constraints, however with large inter-story drift values in the lower half of the structure. The displacements are over-compensated, see also Fig. 5 (b). The influence of the few actuators is limited such that the optimal displacement form cannot be

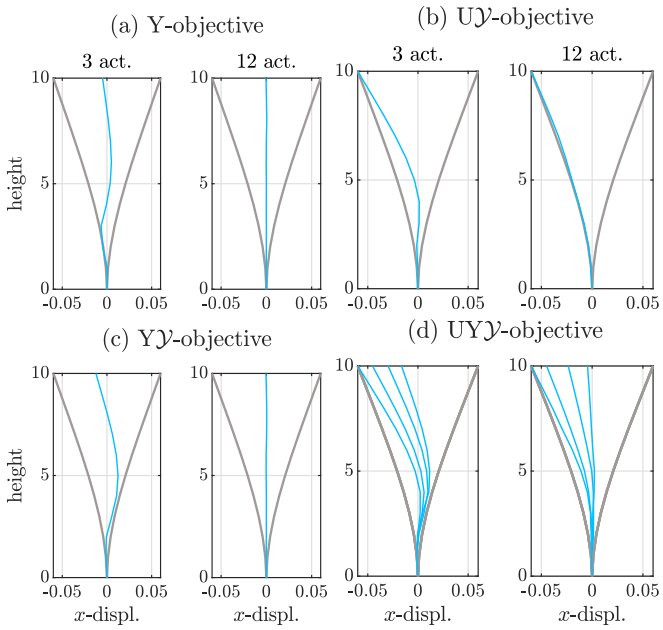

Fig. 7. Side slopes for three and 12 placed actuators for load from the right for the (a) Y-, (b) U$\mathcal{Y}$-, (c) Y$\mathcal{Y}$- and (d) UY$\mathcal{Y}$-objective.

reached. The resulting actuator configurations are depicted in Fig. 6 (b). The selection of actuators shows a pattern: as the number of actuators increases, actuators are placed from bottom to top, beginning with the vertical columns. With only a few placed actuators, the lower vertical columns are used to bend the structure towards the upwind side such that the displacements at the top are just within the constraints. For an increasing number of actuators, some more columns are chosen approximately up to the vertical center. After this, diagonals are chosen for actuation from top to bottom, with some more vertical columns included in between.

c) Y$\mathcal{Y}$-Objective: When using this objective, for more than five actuators, the displacement constraints are inactive. As expected, results similar to those for using the Y-objective are obtained. The displacements and actuator forces norms are the same up to numerical inaccuracies, see Fig. 5 (c) as well as the side line for 12 actuators, see Fig. 7 (c). For five or less actuators, the displacement constraints at the bottom of the structure are active leading to slightly larger displacements and slightly smaller actuator forces in comparison to those for using the Y-objective. The side line for three actuators is in the lower part similar to that of the U$\mathcal{Y}$-objective. In comparison to the Y-objective, the displacement constraints lead to a smaller curvature in the lower part meaning less inter-story drift. The selection of actuators (see Fig. 6 (c)) does not show a clear pattern compared to the U$\mathcal{Y}$-objective. However, generally speaking, lower story columns are chosen before upper story columns, and diagonals in the vertical center are chosen very late.

d) UY$\mathcal{Y}$-Objective: The actuator forces and displacements for using this objective are depicted in Fig. 5 (d) for different weighting factors $\alpha \in \{0.1, 0.5, 0.7, 0.9\}$. The displacements generally increase for increasing α, the actuator forces decrease. The same amount of displacement decrease is approximately achieved by the same amount of actuator force increase. The side lines for three and 12 actuators morph with increasing α from the side lines of the Y$\mathcal{Y}$-objective to the slopes of the U$\mathcal{Y}$-objective, see Fig. 7 (d). Overall, minimizing a weighted sum of the displacements and the actuator forces under displacement constraints leads to results that are a trade-off between those obtained when optimizing only one. This trade-off is also evident in the resulting actuator configurations for $\alpha = 0.5$ in Fig. 6 (d). The pattern of the U$\mathcal{Y}$ target is discernible, but interrupted for some number of actuators.

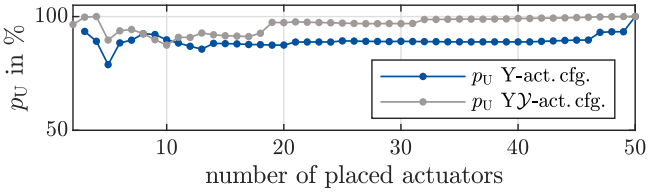

Fig. 8. Performance values of the Y- and Y$\mathcal{Y}$-actuator configurations w. r. t. to the U$\mathcal{Y}$-objective.

B. Performance of Y$\mathcal{Y}$- and Y-Actuator Configurations with respect to the U$\mathcal{Y}$-Objective

As elaborated above, the Y-, U$\mathcal{Y}$- and Y$\mathcal{Y}$-objectives lead to different actuator configurations as shown in Fig. 6. To investigate the suitability of the the actuator configurations obtained for optimizing the Y- and Y$\mathcal{Y}$-objectives for the U$\mathcal{Y}$-objective, they are reevaluated w. r. t. the U$\mathcal{Y}$-objective. The inner OP (6) is solved using $J(\boldsymbol{U}, \boldsymbol{Y}) = J_{\mathrm{U}\mathcal{Y}}$ for the Y- and Y$\mathcal{Y}$-actuator configurations, respectively. The resulting actuator forces $\boldsymbol{U}^*_{\mathrm{Y}}$ and $\boldsymbol{U}^*_{\mathrm{Y}\mathcal{Y}}$ are related to those obtained for the U$\mathcal{Y}$-actuator configurations by the performance measure

$$p_\mathrm{U} = \left(1 - \frac{\boldsymbol{U}^* - \boldsymbol{U}^*_{\mathrm{U}\mathcal{Y}}}{\boldsymbol{U}^*_{\mathrm{U}\mathcal{Y}}}\right) \text{ with } \boldsymbol{U}^* \in \{\boldsymbol{U}^*_{\mathrm{Y}}, \boldsymbol{U}^*_{\mathrm{Y}\mathcal{Y}}\}. \quad (7)$$

For the Y$\mathcal{Y}$-actuator configurations, Fig. 8 reveals that the performance is 95 % on average, which means that the Y$\mathcal{Y}$-actuator configurations require 5 % higher actuator forces to maintain the displacement constraints than the U$\mathcal{Y}$-actuator configurations. The the Y-actuator configurations require on average 12 % higher actuator forces. This illustrates the impact of the design of an adaptive structure, including the actuator configuration, on the performance or actuator force demand during operation, which is significant, but within reasonable ranges here.

C. Impact of Loads

This section analyzes how well actuator configurations optimized for other loads perform for the two loads used previously. First, the OP (5) is solved using $J(\boldsymbol{U}, \boldsymbol{Y}) = J_{\mathrm{U}\mathcal{Y}}$ with only one of the static wind loads. Interestingly, the results are the same as for the optimization with both static wind loads. So the solution of the inner OP (6) for only one of the loads equals the solution of the multi-objective inner OP (6) for two loads. This property is explained by the symmetry of the considered structure and may not hold for arbitrary structures. Future research will investigate, which structure characteristics lead to this property, since optimizing for less loads reduces the computational effort,

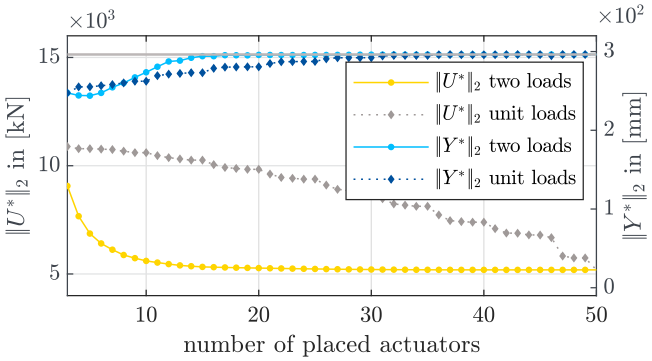

Fig. 9. Norm of actuator forces and displacements for the U$\mathcal{Y}$-objective with two loads for actuator configurations optimized with two loads and unit loads, respectively.

what is important, when placing actuators in larger structures consisting of much more elements.

Second, the OP (5) is solved using $J(\boldsymbol{U}, \boldsymbol{Y}) = \mathrm{U}\mathcal{Y}$ with a unit load, as used in previous work: $\boldsymbol{E}$ is chosen as the identity, the amplitudes $\boldsymbol{z}$ are chosen to be 1000. The resulting actuator configurations show a pattern: actuators are placed from top to bottom, see Fig. 6 (e). The two dark colored lower column actuators were manually excluded during the optimization. The resulting actuator configurations are reevaluated w. r. t. U$\mathcal{Y}$-objective and the two static wind loads. If the two lower column actuators were not excluded from the simulation, the inner OP (6) would only be solvable for more than 45 actuators. While the resulting displacements are in the same range, see Fig. 9, the actuator forces are significantly larger than for the actuator configurations optimized for the two static wind loads. This illustrates the importance of using realistic load cases.

V. Summary and Conclusion

For adaptive structures subject to static loads, a general two-stage actuator placement optimization procedure is introduced. The optimal actuator forces related to an actuator configuration are calculated by solving an inner OP, while an outer OP optimizes over the actuator configurations based on the solution of the inner OP. Using this procedure, actuators are placed into a structure subject to static wind loads such that the actuator forces required to reach certain displacement constraints (maximum displacement and inter-story drift) are minimum. For comparison, three more objectives are studied: minimization of displacements with and without considering the displacement constraints as well as minimization of the weighted sum of displacements and actuator forces under the displacement constraints. For each objective the resulting displacements and actuator forces norms converge towards a limit, here reached from about 10 to 15 actuators. When minimizing the actuator forces while reducing the displacements only to satisfy the displacement constraints, around 40 % smaller actuator forces are needed compared to those necessary for displacement minimization. When using a weighted sum of displacements and actuator forces as objective, the results are in-between. Regarding the resulting actuator configurations, a pattern results when minimizing the actuator forces (vertical lower columns are placed first), in contrast to displacement minimization, where actuators are placed distributed over the structure. The actuator configurations optimized for displacement minimization perform between 5 % and 12 % less good w. r. t. actuator force minimization than actuator configurations optimized for that. To study the impact of the used loads on the optimization results, actuator configurations were optimized (minimization of actuator forces) for unit loads. The resulting actuator configurations are different to those optimized for static wind loads and under static wind loads they perform significantly worse than the actuator configurations optimized for static wind loads.

Future research will evaluate the actuator placement objectives for more complex structures and use the D1244 high-rise to validate the results of this work. Furthermore, the impact of the loads and of other constraints, such as actuator force limits, will be systematically studied.

References

[1] L. Blandini et al. “D1244: Design and Construction of the First Adaptive High-Rise Experimental Building”. In: *Front. Built Environ.* (2022).

[2] P. Teuffel and W. Sobek. “Adaptive systems in architecture and structural engineering”. In: *Smart Structures and Materials* (2001).

[3] Y. Wang and G. Senatore. “Design of adaptive structures through energy minimization: extension to tensegrity”. In: *Struct. Multidiscipl. Optim.* (2021).

[4] F. Schlegl et al. “Integration of LCA in the Planning Phases of Ad. Buildings”. In: *Sustainability* (2019).

[5] J. L. Wagner et al. “On steady-state disturbance compensability for actuator placement in adaptive structures”. In: *at-Automatisierungstechnik* (2018).

[6] M. Heidingsfeld et al. “Gramian-based Actuator Placement with Spillover Reduction for Active Damping of Adaptive Structures”. In: 2017.

[7] G. Senatore and A. Reksowardojo. “Force and shape control strategies for minimum energy adaptive structures”. In: *Front. Built Environ.* (2020).

[8] Y. Wang and G. Senatore. “Minimum energy adaptive structures – All-In-One problem formulation”. In: *Computers and Structures* (2020).

[9] M. Böhm et al. “Homogenizability of element utilization in adaptive structures”. In: 2019.

[10] M. Böhm et al. “Input modeling for active structural elements-extending the established FE-Workflow for modeling of adaptive structures”. In: 2020.

[11] E. Gladin et al. “Solving Smooth Min-Min and Min-Max Problems by Mixed Oracle Algorithms”. In: 2021.

[12] *Numerical Optimization*. Springer New York, 2006.

[13] A. Zeller, M. Böhm, and O. Sawodny. “A Genetic and a Greedy-Genetic Algorithm for Steady-State Disturbance Compensability Actuator Placement for Adaptive Structures”. In: *2022 American Control Conference*. 2022.